#### Log Number: 347

# NUMERICAL SIMULATION OF FLOW AND THERMAL FIELD IN SUPERCRITICAL PRESSURE CARBON DIOXIDE FLOWING UPWARD IN A NARROW TUBE

#### Y. Y. Bae, S. D. Hong, Y. W. Kim

Korea Atomic Energy Research Institute, 1045 Daedeokdaero, Daejeon, Republic of Korea <a href="mailto:yybae@kaeri.re.kr">yybae@kaeri.re.kr</a>, <a href="mailto:sdhong1@kaeri.re.kr">sdhong1@kaeri.re.kr</a>, <a href="mailto:ywkim@kaeri.re.kr">ywkim@kaeri.re.kr</a>

#### **Abstract**

A reliable heat transfer correlation valid at a supercritical pressure is indispensible for an accurate estimation of heat transfer in the sub-channel of a fuel assembly of Supercritical Water-Cooled Reactors (SCWR). Despite a number of supercritical heat transfer correlations having been proposed in the past several decades, a reliable one is still missing, since the predictions by the existing correlations show wide discrepancies from each other. In a mixed convection regime, no correlation is able to produce accurate predictions. Under the influence of strong buoyancy, the boundary layer structure is known to deform significantly, when the wall temperature is close to the pseudo-critical temperature; and, therefore, it is suspected to be one of the reasons for the enhancement or impairment of the heat transfer rate. However, a detailed analysis of the boundary-layer transformation process has never been successfully addressed, due partially to difficulty in experimenting at a condition of high pressure and temperature, and to an inadequacy of the numerical tools in dealing with substantial property variations. This paper provides results of the numerical analyses of flow and thermal field in CO<sub>2</sub> flowing upward in a narrow tube.

#### 1. Introduction

Since the Supercritical Pressure water Cooled Reactor (SCWR) was selected as one of the candidates for Generation IV reactors [1], heat transfer at a supercritical pressure has been considered as one of the most important research areas. In the past a number of correlations have been proposed by various researchers, but most are valid only in a forced convection regime as shown in the review papers by Cheng and Schulenberg [2] and Pioro and Duffey [3]. The correlations reported in the papers predicted heat transfer rate with a reasonable accuracy in a forced convection regime. However, in a mixed convection regime, such correlation was not able to produce accurate predictions. In this context, many efforts have been given to formulate reliable correlations for mixed convection heat transfer by Watts and Chou [4] and Jackson and Hall [5], Jackson et al. [6], Bae and Kim [7], Bae et al. [8], Bae [9], and Jackson [10].

In addition to the experiments, a number of numerical approaches have been performed to investigate the flow and thermal field of flow at supercritical pressure. For both forced and mixed convection regimes, experimental and numerical investigations of thermal and flow field at supercritical pressure was performed by Licht et al. [11]. They confirmed that for the simple case of deterioration investigated in detail, FLUENT (a commercial CFD code) simulations offered qualitative insight into changes in fluid temperature and turbulent velocities responsible for the axial evolution of the wall temperature. Cho et al. [12] examined three turbulence models against experimental data obtained for a tube and annulus with a equivalent hydraulic diameter of 4.4 mm and reported that the performance of the three models was partially successful. He et

al. [13] thoroughly investigated low-Reynolds number turbulence models and concluded that both the low Reynolds number k- $\varepsilon$  models and the V2F models were able to capture the general trends of the interesting wall temperature behaviour observed with upward flow in some experiments with a fluid at a pressure just above the critical value, while the detailed variation of the wall temperature predicted by using each model was rather different from that in the experiments. They also found that the effect on heat transfer seen was almost entirely due to the shear production effect caused by the distortion of the mean flow as a result of the strong influence of buoyancy. Zhang et al. [14] successfully reproduced the data from a DNS calculation and an experiment by employing algebraic flux model [Eq. (9)] in calculating the turbulence production by buoyancy. However, its application to the other conditions is still to be proven.

In this paper, the low-Reynolds number turbulence models will be applied in the calculation of thermal and flow field, which will be examined against the available DNS data, focusing on the influence of buoyancy.

#### 2. Numerical method

# 2.1 Governing equations and turbulence model

In the present study a vertically upward flowing fluid in a uniformly heated tube was considered. The flow was assumed to be steady 2-D axi-symmetric. The vertical upward direction was aligned with positive x direction and the radial coordinate was r. The governing equations employed in the present study were the continuity equation, ensemble averaged Navier-Stokes equation, energy equation, two equation models for turbulent kinetic energy and temperature fluctuation. The governing equations for velocity field in a cylindrical coordinate with two-equation k- $\varepsilon$  turbulence model read:

$$\frac{1}{r} \left\{ \frac{\partial}{\partial x} \left( r \overline{\rho} \overline{u} \right) + \frac{\partial}{\partial r} \left( r \overline{\rho} \overline{v} \right) \right\} = 0 \tag{1}$$

$$\frac{1}{r} \left\{ \frac{\partial}{\partial x} \left( r \overline{\rho} \overline{u}^{2} \right) + \frac{\partial}{\partial r} \left( r \overline{\rho} \overline{u} v \right) \right\} = -\frac{\partial p}{\partial x} + \overline{\rho} g_{x} + \frac{2}{r} \frac{\partial}{\partial x} \left[ r \mu_{e} \left( \frac{\partial \overline{u}}{\partial x} \right) \right] + \frac{1}{r} \frac{\partial}{\partial r} \left[ r \mu_{e} \left( \frac{\partial \overline{u}}{\partial r} + \frac{\partial \overline{v}}{\partial x} \right) \right] \tag{2}$$

$$\frac{1}{r} \left\{ \frac{\partial}{\partial x} \left( r \overline{\rho} \overline{u} \overline{v} \right) + \frac{\partial}{\partial r} \left( r \overline{\rho} \overline{v}^{2} \right) \right\} = -\frac{\partial p}{\partial r} + \overline{\rho} g_{r} + \frac{1}{r} \frac{\partial}{\partial x} \left[ r \mu_{e} \left( \frac{\partial \overline{v}}{\partial x} + \frac{\partial \overline{u}}{\partial r} \right) \right] + \frac{2}{r} \frac{\partial}{\partial r} \left[ r \mu_{e} \left( \frac{\partial \overline{v}}{\partial r} \right) \right] - 2 \frac{\mu_{e} \overline{v}}{r^{2}} \tag{3}$$

$$\frac{1}{r} \left\{ \frac{\partial}{\partial x} \left( r \overline{\rho} \overline{u} k \right) + \frac{\partial}{\partial r} \left( r \overline{\rho} \overline{v} k \right) \right\} = \frac{\partial}{\partial x} \left[ \left( \overline{\mu} + \frac{\overline{\mu}_t}{\sigma_k} \right) \frac{\partial k}{\partial x} \right] + \frac{1}{r} \frac{\partial}{\partial r} \left[ r \left( \overline{\mu} + \frac{\overline{\mu}_t}{\sigma_k} \right) \frac{\partial k}{\partial r} \right] + \rho P_k + \rho G_k - \overline{\rho} \varepsilon$$
 (4)

$$\frac{1}{r} \left\{ \frac{\partial}{\partial x} \left( r \overline{\rho} \overline{u} \varepsilon \right) + \frac{\partial}{\partial r} \left( r \overline{\rho} \overline{v} \varepsilon \right) \right\} = \frac{\partial}{\partial x} \left[ \left( \overline{\mu} + \frac{\overline{\mu}_{t}}{\sigma_{\varepsilon}} \right) \frac{\partial \varepsilon}{\partial x} \right] + \frac{1}{r} \frac{\partial}{\partial r} \left[ r \left( \overline{\mu} + \frac{\overline{\mu}_{t}}{\sigma_{\varepsilon}} \right) \frac{\partial \varepsilon}{\partial r} \right] + \overline{\rho} C_{\varepsilon 1} f_{\varepsilon 1} \frac{\varepsilon}{k} \left( P_{k} + C_{\varepsilon 3} G_{k} \right) - \overline{\rho} C_{\varepsilon 2} f_{\varepsilon 2} \frac{\varepsilon^{2}}{k} \right]$$
(5)

where  $\mu_e$  is the effective viscosity defined by  $\mu_e = \overline{\mu} + \overline{\mu}_t$ , and  $\overline{\mu}_t$  the turbulent viscosity, which is defined as

$$\overline{\mu}_{t} = \overline{\rho} C_{\mu} f_{\mu} \frac{\overline{k}^{2}}{\overline{\varepsilon}} \tag{6}$$

in which  $f_{\mu}$  is a damping function to account for the near-wall effect and  $C_{\mu}$  is a constant. The turbulent stress  $-\overline{\rho u_i v_j}$  was modelled by the Boussinesque approximation.

$$-\overline{\rho u_i u_j} = \mu_t \left( \frac{\partial u_j}{\partial x_i} + \frac{\partial u_i}{\partial x_j} \right) - \frac{2}{3} \delta_{ij} \overline{\rho k}$$
 (7)

The production of turbulent energy by interaction with the mean flow and turbulence  $P_k$  was defined as

$$P_{k} = \overline{V}_{t} \left[ 2 \left\{ \left( \frac{\partial \overline{u}}{\partial x} \right)^{2} + \left( \frac{\partial \overline{v}}{\partial r} \right)^{2} + \left( \frac{\overline{v}}{r} \right)^{2} \right\} + \left( \frac{\partial \overline{u}}{\partial r} + \frac{\partial \overline{v}}{\partial x} \right)^{2} \right]$$
(8)

The gravitational production  $G_k = \overline{\rho u}g/\rho$  or  $G_k = -\beta g_i \overline{u_i t}$  was modelled by using the algebraic flux model (AFM) [15,16] shown below.

$$\overline{u_i t} = -\frac{u_i u_j \frac{\partial T}{\partial x_j} + (1 - C_{t2}) \overline{u_j t} \frac{\partial u_i}{\partial x_j} + (1 - C_{t3}) \beta g_i \overline{t^2}}{C_{t1} \varepsilon / k}$$
(9)

For a vertical upward flow in a tube  $g_x = -g$  and  $g_r = 0$ .

The governing equations for thermal field in a cylindrical coordinate with two-equation model for thermal field [17] read:

$$\frac{1}{r} \left\{ \frac{\partial}{\partial x} \left( r \overline{\rho} \overline{u} \overline{h} \right) + \frac{\partial}{\partial r} \left( r \overline{\rho} \overline{v} \overline{h} \right) \right\} = \frac{1}{r} \left\{ \frac{\partial}{\partial x} \left[ r \left( \frac{\overline{\mu}}{Pr} + \frac{\overline{\mu}_t}{\sigma_t} \right) \frac{\partial \overline{h}}{\partial x} \right] + \frac{\partial}{\partial r} \left[ r \left( \frac{\overline{\mu}}{Pr} + \frac{\overline{\mu}_t}{\sigma_t} \right) \frac{\partial \overline{h}}{\partial r} \right] \right\} \tag{10}$$

$$\frac{1}{r} \left\{ \frac{\partial}{\partial x} \left( r \overline{\rho} \overline{u} k_{t} \right) + \frac{\partial}{\partial r} \left( r \overline{\rho} \overline{v} k_{t} \right) \right\} = \frac{\partial}{\partial x} \left[ \left( \overline{\lambda} + \frac{\overline{\lambda}_{t}}{\sigma_{h}} \right) \frac{\partial k_{t}}{\partial x} \right] + \frac{1}{r} \frac{\partial}{\partial r} \left[ r \left( \overline{\lambda} + \frac{\overline{\lambda}_{t}}{\sigma_{h}} \right) \frac{\partial k_{t}}{\partial r} \right] + \rho c_{p} P_{t} - \overline{\rho} c_{p} \varepsilon_{t}$$
(11)

$$\frac{1}{r} \left\{ \frac{\partial}{\partial x} \left( r \overline{\rho} \overline{u} \varepsilon_{t} \right) + \frac{\partial}{\partial r} \left( r \overline{\rho} \overline{v} \varepsilon_{t} \right) \right\} = \frac{\partial}{\partial x} \left[ \left( \overline{\lambda} + \frac{\overline{\lambda}_{t}}{\sigma_{\phi}} \right) \frac{\partial \varepsilon_{t}}{\partial x} \right] + \frac{1}{r} \frac{\partial}{\partial r} \left[ r \left( \overline{\lambda} + \frac{\overline{\lambda}_{t}}{\sigma_{\phi}} \right) \frac{\partial \varepsilon_{t}}{\partial r} \right] + \overline{\rho} c_{p} C_{p_{1}} f_{p_{1}} \frac{\varepsilon_{t}}{k_{t}} P_{t} + \overline{\rho} c_{p} C_{p_{2}} f_{p_{2}} P_{k} \frac{\varepsilon_{t}}{k} - \overline{\rho} c_{p} C_{p_{2}} f_{p_{2}} P_{k} \frac{\varepsilon_{t}}{k} \right] - \overline{\rho} c_{p} C_{D_{1}} f_{D_{1}} \frac{\varepsilon_{t}^{2}}{k_{t}} P_{t} - \overline{\rho} c_{p} C_{D_{2}} f_{D_{2}} \frac{\varepsilon \varepsilon_{t}}{k}$$

$$(12)$$

where  $\overline{Pr}$  is the molecular Prandtl number and  $\sigma_t$  is the turbulent Prandtl number. The over bar represents a time averaging. The turbulent Prandtl number  $\sigma_t$  is set as 0.9 as suggested by Myong et al. [18] after extensive computational experiment for a turbulent pipe flow. They suggested that  $\sigma_t$  is practically unity unless Pr is far smaller than unity. The turbulent heat flux  $-\overline{\rho u_t t}$  were also modelled by the Boussinesque approximation.

$$-\overline{\rho u_i h} = \frac{\mu_i}{\sigma_i} \frac{\partial h}{\partial x_i} \tag{13}$$

The temperature fluctuation,  $k_t$ , and its dissipation rate,  $\varepsilon_t$ , was defined as  $\overline{t^2}$ ,  $\alpha(\partial t/\partial x_i)(\partial t/\partial x_i)$ , respectively.

The constants for the turbulence model are summarized in Table 1. The constants are the same as those proposed by Zhang et al. [14] except for the constant for buoyancy attribution  $C_{\varepsilon_3}$ .

Table 1 Constants in the turbulence model

$C_{\mu}$	$C_{arepsilon 1}$	$C_{arepsilon 2}$	$C_{\varepsilon 3}$	$\sigma_{\scriptscriptstyle k}$	$\sigma_{arepsilon}$	$f_{arepsilon 1}$	$C_{P1}$
0.09	1.42	1.8	1.0	1.4	1.4	1.0	0.95
$f_{P1}$	$f_{P2}$	$C_{\scriptscriptstyle D1}f_{\scriptscriptstyle D1}$	$\sigma_{\scriptscriptstyle h}$	$\sigma_{\scriptscriptstyle{\phi}}$	$C_{t1}$	$C_{t2}$	$C_{t3}$
1.0	1.0	1.1	1.6	1.4	1.5	0.33	0.33

The model functions in the two-equation models were defined as follows.

$$f_{\mu} = \left(1 + \frac{5}{R e_t^{0.75}}\right) \left[0.7 + 0.5 \exp\left(-\frac{Re_b}{15000}\right)\right] \left\{1 - \exp\left[-\left(\frac{y^+}{40}\right)^2\right]\right\}$$
(14)

$$f_{\varepsilon 2} = \left[1 - 0.3 \exp\left(-Re_t^2\right)\right] \left[1 - \exp\left(-\frac{y^+}{5.5}\right)\right]^2 \tag{15}$$

$$C_{P2} = 0.62 + 1.2 \exp(-3.2Pr)$$
 (16)

$$C_{D2}f_{D2} = \left\{ C_{\varepsilon 2} \left[ 1 - 0.3 \exp\left(-Re_t^2\right) \right] - 1 \right\} \left[ 1 - \exp\left(-\frac{y^+}{5.5}\right) \right]^2$$
 (17)

In order to incorporate the effect of Reynolds number variation due to property variation along the tube, the second term of the product on the right hand side of the damping function given by Eq. (14) was added to the widely used ones [19,20,21,22]. Please note that in the region very near a wall,  $f_{\mu} \propto 1/y^+$ . In Eq. (14), the first term of the product on the right hand side represents the change of the length scale for the dissipation rate at low and high turbulent Reynolds numbers, and the third term the ratio of the length scale for turbulent momentum transport to that for dissipation rate [21]. Under the constraint of mass conservation,  $-uv \propto y^3$ ,  $k \propto y^2$ , and  $\varepsilon \to \varepsilon_w$  as  $y \to 0$ , the Kolmogorov-Prandtl relationship requires that  $f_{\mu} \propto y^{-1}$ [23].

The boundary conditions were:

$$\frac{\partial \overline{u}}{\partial x} = \frac{\partial \overline{v}}{\partial x} = \frac{\partial \overline{h}}{\partial x^2} = \frac{\partial k}{\partial x} = \frac{\partial \varepsilon}{\partial x} = \frac{\partial k_t}{\partial x} = \frac{\partial \varepsilon_t}{\partial x} = 0 \text{ at the outlet:}$$
 (18a)

$$\overline{u} = \overline{v} = k = \frac{\partial \varepsilon}{\partial r} = \frac{\partial k_t}{\partial r} = \frac{\partial \varepsilon_t}{\partial r} = 0$$
 at the wall: (18b)

$$\frac{\partial \overline{u}}{\partial x} = \frac{\partial \overline{v}}{\partial x} = \frac{\partial \overline{h}}{\partial x} = \frac{\partial k}{\partial x} = \frac{\partial \varepsilon}{\partial x} = 0$$
 at the symmetry line (18c)

The boundary condition for  $\varepsilon$  at the wall was set as  $\partial \varepsilon / \partial r = 0$  as suggested by Patel at al. [24] and Herrero et al. [25]. The well known boundary condition,  $\varepsilon_w = 2\nu k_1/n_1^2$ , resulted in a unrealistically large value, while the present boundary condition resulted in a reasonable value of  $\varepsilon_w$ .

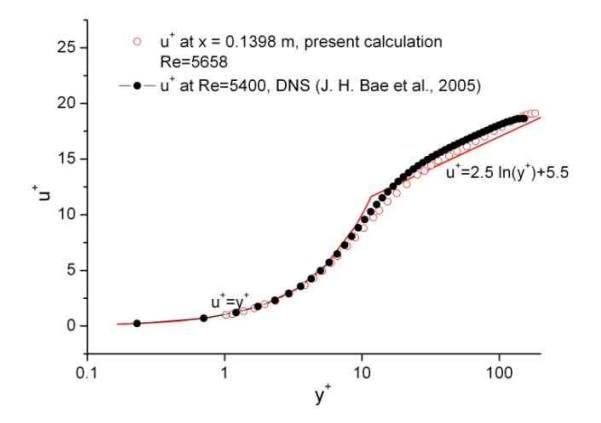
# 2.2 Numerical procedure

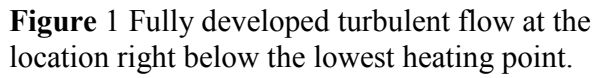
The present computational study was performed by using an in-house code, a version modified from the one provided by Ferziger and Peric [26]. Basically the SIMPLE algorithm with a single pressure correction step was applied. All variables were assigned to collocated grids. Diffusive fluxes were discretized using central differences; while, for convective fluxes, linear interpolation was allowed to be blended with an upwind approximation. The resulting matrix of the variables was iteratively solved by the Stone's SIP (strongly implicit procedure) method. The computational object was a vertical upward flow of carbon dioxide in a uniformly heated circular tube with an inner diameter of 2.0 mm. The flow conditions at the inlet were 301°K, 8.0 MPa, and 166.62 kg/m²s. To obtain a fully developed turbulent velocity distribution before fluid reaches the lower end of heated section, a velocity distribution proportional to a 1/7 power of reduced radius was assumed at the tube entrance. A sufficiently long flow developing region with a length of 0.14 m was provided in front of the heated section to ensure a fully developed turbulent flow at the entrance of heated section of 0.06 m under a constant heat flux of 30.87 kW/m², which corresponds to the domain of the DNS calculation performed by Bae et al. [27],

which is supposed to be compared with the present results. The calculation domain was discretized into an orthogonal grid of 50 (radial) x 150 (axial). The grid was refined towards the entrance of heated section in axial direction, and into the wall in radial direction. After trying several values of  $y_P^+$  (the value of  $y^+$  at the first node from the wall),  $y_P^+ < 0.5$  was found to be optimum with a result of reasonably accurate converged solutions. The mesh refining function, an exponential function, was revised whenever  $y_P^+$  became greater than 0.5, in order to secure  $y_P^+ < 0.5$  for all calculations.

The pressure term in the calculation was actually the head including the hydrostatic pressure, that is,  $\tilde{p} = p + \rho_0 gh$ . The difference between  $p + \int_{z=0}^{z=h} \rho g dz$  and  $p + \rho_0 gh$ ,  $\int_{z=0}^{z=h} (\rho - \rho_0) g dz$ , was treated as a buoyancy term in the momentum equation. The actual pressure drop due to skin friction was obtained by subtracting hydrostatic pressure from  $\tilde{p}$ . The  $\Delta p$  due to skin friction was found to be about 1500 Pa. Such a small pressure drop will not affect the fluid properties in a practical sense and it justifies the assumption made here that the properties vary only with temperature. The fluid properties were calculated from a table constructed from the NIST standard reference database [28] for the interval,  $220^{\circ}\text{K} < T < 800^{\circ}\text{K}$ , with  $\Delta T = 1.0$ , while for the steep property-varying interval,  $292^{\circ}\text{K} < T < 318^{\circ}\text{K}$ ,  $\Delta T = 0.1$ . The fluid properties were obtained by a linear interpolation.

The grid independence was indirectly confirmed by comparing the non-dimensional mean axial velocity and the Nusselt numbers obtained from the present calculation with those from the DNS data [27] as shown in Figure 1 and Figure 2. The mean velocity distribution showed a good agreement with the DNS data. The Nusselt number also agreed with the DNS data reasonably, although not exactly, particularly in the regions of commencement of heating and near the exit plane. However, it qualitatively proved that the current work showed a capability of capturing the phenomena occurring in a narrow tube at a supercritical pressure, both dynamically and thermally.





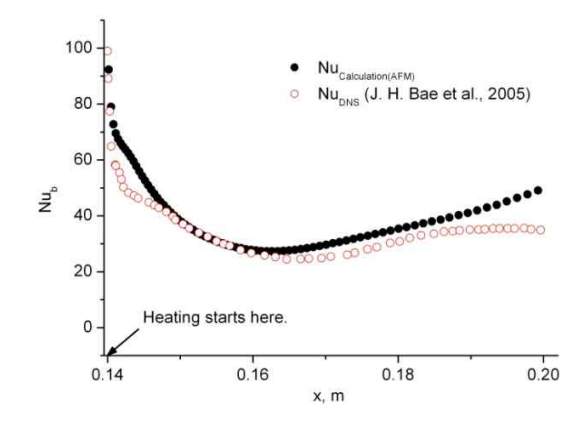


**Figure** 2 Streamwise distribution of the local Nusselt number.

# 3. Results of calculation

Figure 3 shows the comparison between the calculations with and without the two-equation model for thermal field. It can be seen that the calculation with the latter excellently agreed with the DNS calculation, while the result without the former highly over-estimated the wall temperature.

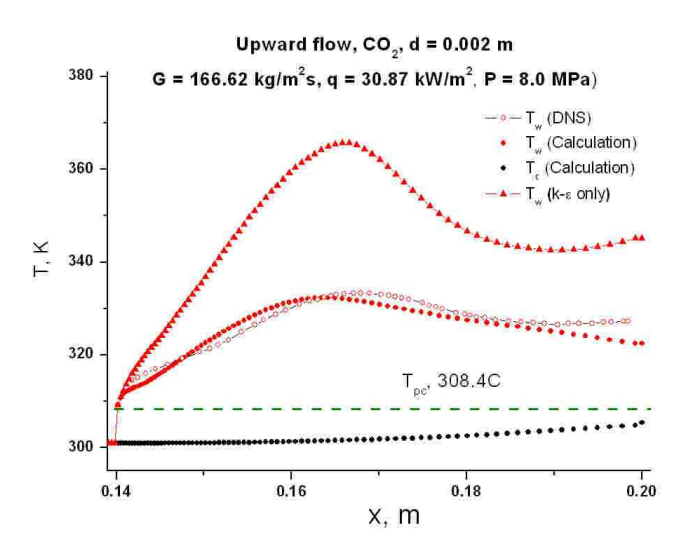


Figure 3 Wall and bulk temperature distribution along the tube wall.

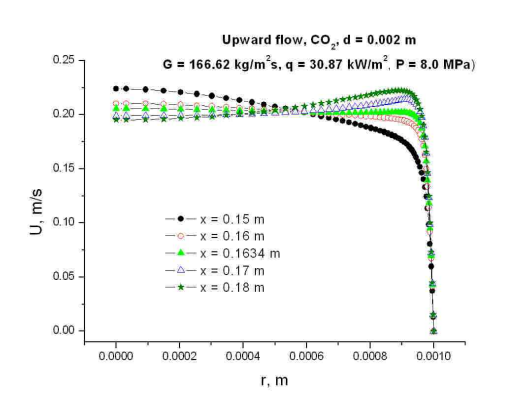
The velocity distributions across the tube cross section at several axial locations are shown in Figure 4. At x = 0.15 axial velocity retained a typical distribution of turbulent flow. The flattening of the velocity distribution already appears at x = 0.16: and it eventually developed into an M-shape distribution at x = 0.1634, where the wall temperature showed the maximum. As the flow advanced further downstream the shoulder of M heightened; and it was the most conspicuous at x = 0.18. If the flow travels downstream sufficiently, the velocity distribution will recover the typical distribution for turbulent flow, for the density across the whole cross section becomes uniform at low density.

The temperature distribution in Figure 5 shows that the temperature gradients near the wall was very large, indicating that the heat did not dissipate efficiently. At around the wall temperature peak the high temperature region was restricted near the wall, while the bulk temperature showed gradual increase along the tube.

The distributions of specific heat are shown in Figure 6. The point of the maximum specific heat was located off the wall when its temperature showed a peak. Beyond the point of the maximum wall temperature, as the wall temperature decreased, the peak point of specific heat moved back towards the wall, resulting in a reduction of the low density layer thickness. It indicates that the sudden increase of the wall temperature partially, at least, might have resulted from heat transfer impairment due the low density layer near the wall.

Another important factor for heat transfer deterioration is a reduction of shear stress and consequent decrease of eddy diffusivity, as is evident in Figure 7. At x = 0.15 the shear stress

reduction already was apparent in the region near the wall, which otherwise showed a linear decrease from the wall the symmetry line as shown at x = 0.14, a point located immediately ahead of the entrance of the heated section. The reduction of shear stress continued as expected from the M-shape velocity distribution in the region x > 0.1634.



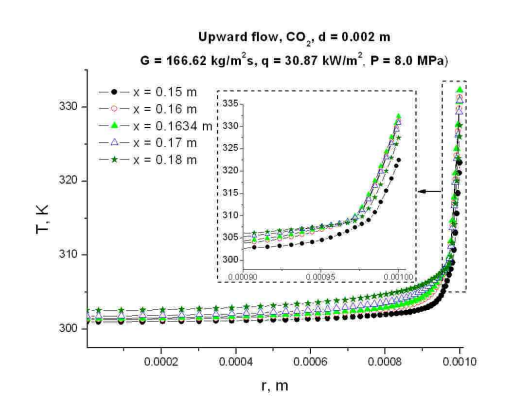
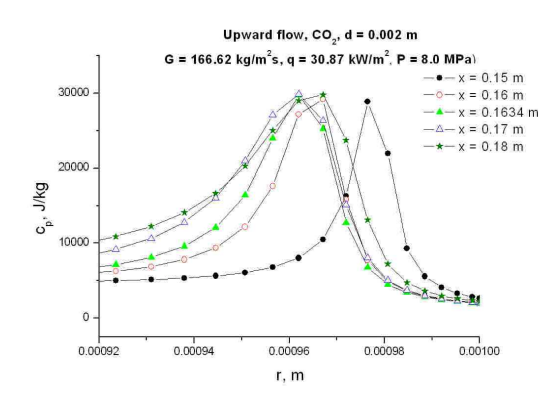


Figure 4 Velocity.

Figure 5 Temperature.



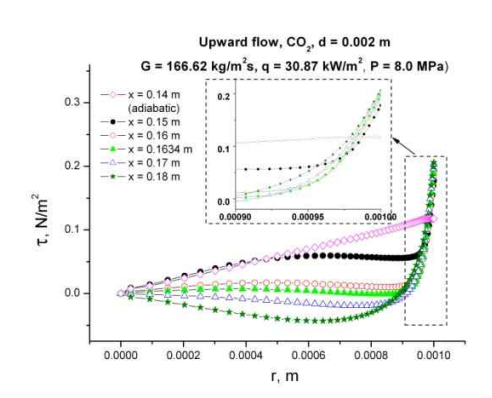


Figure 6 Specific heat.

Figure 7 Shear stress.

Figures 8-11 show the normalized turbulence quantities in velocity field. The turbulent kinetic energy showed two peaks (Figure 8), which probably resulted from the high heat flux from the wall and the consequential influence of buoyancy. The turbulent kinetic energy decreased across the entire cross section until fluid reached x = 0.16 and began to monotonically increase as it flowed further downstream. This initial decrease in turbulent kinetic energy has nothing to do with any physical phenomenon; but purely arose from the reduction of the value of  $u_{\tau}$  in the denominator. The same thing goes to the other turbulent properties. The dissipation rate of turbulent kinetic energy showed a quite similar trend, which was shown in the turbulent kinetic energy; however, it did not show the double peaks (Figure 9). The peak value of the production of turbulent kinetic energy  $P_k$  continuously increased as the fluid travelled downstream (Figure 10), except at the location of x = 0.15. The region of high production of turbulent kinetic energy along the heated section became narrower compared with that along the unheated section. This phenomenon can be explained by the appearance of M-shape velocity distribution, where the region of large radial velocity gradient was more pushed toward the wall; and beyond this region

the velocity distribution flattened and resulted in a low turbulence production. The production of turbulent energy due to buoyancy  $G_k$  also continuously increased as the flow advanced downstream (Figure 11). It should be noted that the values of  $G_k$  were twice as larger as  $P_k$ , showing a significant influence of buoyancy to the production of turbulent kinetic energy.

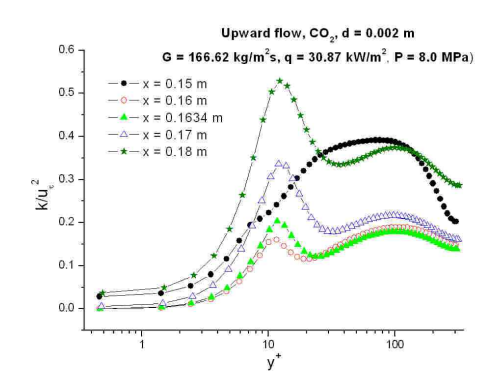
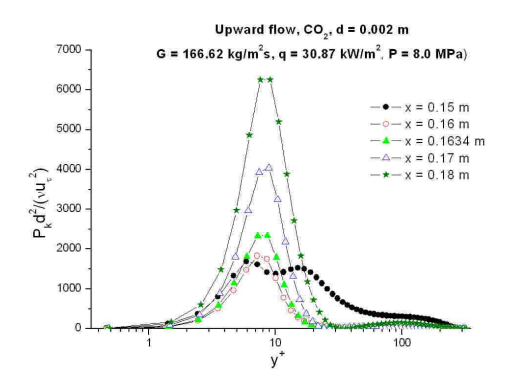


Figure 8 Turbulent kinetic energy.

Figure 9 Dissipation rate of turbulent kinetic energy.



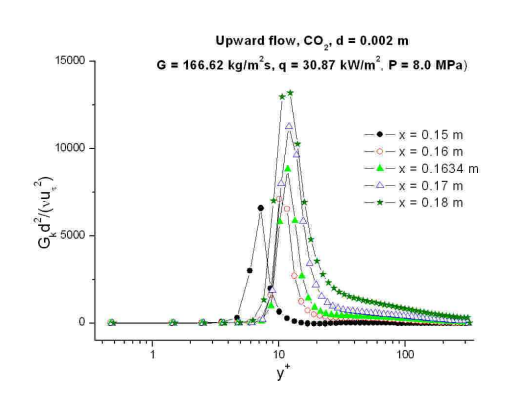


Figure 10 Turbulent kinetic energy production.

Figure 11 Turbulent kinetic energy production due to buoyancy.

The normalized turbulence quantities in thermal field are plotted in Figures 12-14. The variance of temperature fluctuation  $k_t$  continuously increased downstream (Figure 12). This seems natural, considering that a high temperature resulted in a high temperature fluctuation. On the contrary, the dissipation rate of temperature fluctuation continuously decreased downstream (Figure 13). While the temperature fluctuation continuously decreased toward the symmetry line, its dissipation rate increased. The production of temperature fluctuation  $P_t$  continuously increased along the axial direction, showing a very similar radial distribution to that of  $P_k$  and  $G_k$ . (Figure 14).

The eddy diffusivity, -uv, showed a maximum at a relatively large value of  $y^+$ , which appeared due to the flattening of the velocity distribution under the influence of strong buoyancy and the

effect of low-Reynolds number turbulence model (Figure 15). On the other hand the eddy diffusivity for heat showed peaks near the wall and another one at large value of  $y^+$  (Figure 16).

As already indicated, the damping functions shown in Figure 17 was not monotonic, but it varies as 1/y near the wall at the locations x = 0.16 and x = 0.1634, where the wall temperature approached the maximum value.

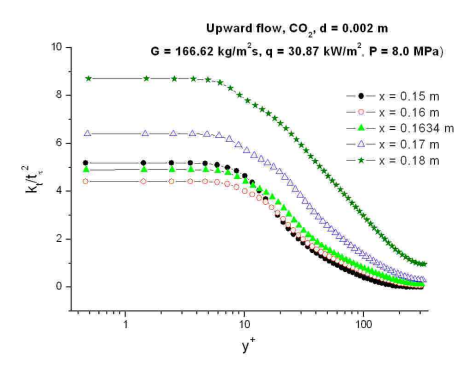


Figure 12 Temperature fluctuation.

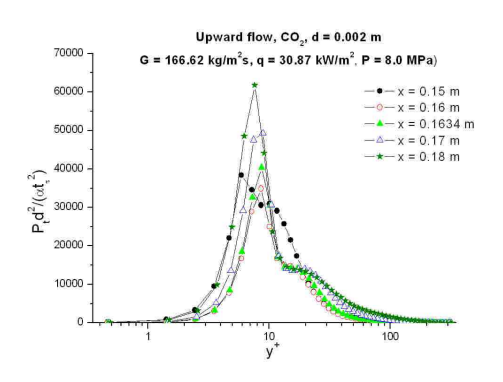


Figure 14 Production of temperature fluctuation.

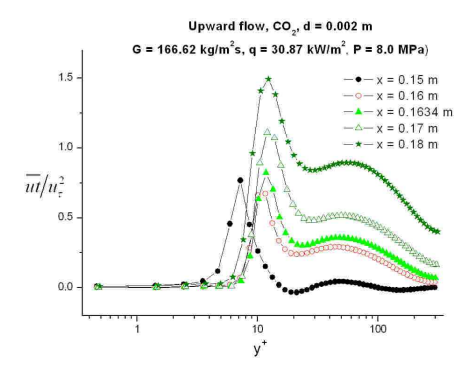


Figure 16 Eddy diffusivity for heat.

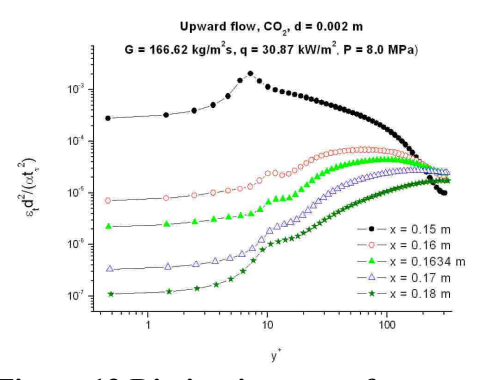


Figure 13 Dissipation rate of temperature fluctuation.

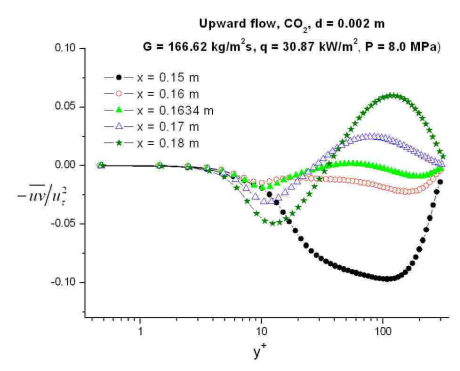


Figure 15 Eddy diffusivity (Reynolds stress).

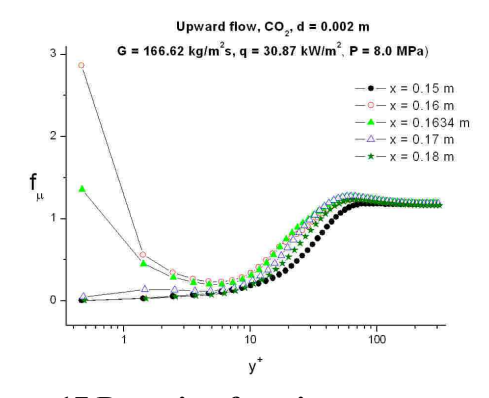


Figure 17 Damping function.

# 4. Conclusion

A numerical simulation of the upward flow of  $CO_2$  in a narrow circular tube has been carried out at a condition of heat transfer deterioration. The introduction of two-equation model for thermal field is considered as one factor for its success. Various flow and thermal as well as turbulence properties were evaluated. For the next step, the numerical simulation will be extended to the conditions where experimental data are available.

# 5. Acknowledgement

The useful communication with Mr. Hao Zhang was of great help for the completion of this paper.

#### 6. Nomenclature

o. Nomenciature				
$C_{Pl}, C_{P2}, C_{Dl}, C_{D2}$ constants in transport equation for $\varepsilon_t$	$u_{\tau}$ friction velocity, $\sqrt{ \tau_{w} /\rho}$ x, axial coordinate			
$C_{\mu}$ $C_{\varepsilon l}$ , $C_{\varepsilon 2}$ constants in transport equation	1 1			
for $\varepsilon$	$y$ distance from wall $y^+$ non-dimensional distance from wall			
$C_{tl}$ , $C_{t2}$ , $C_{t3}$ constants in algebraic flux model	7			
$c_p$ specific heat	() average quantity			
d tube diameter				
$f_{\mu}$ , $f_{\varepsilon l}$ , $f_{\varepsilon 2}$ functions in velocity field	Greek symbols			
turbulence model	$\alpha$ , $\alpha_t$ molecular and eddy diffusivity for			
$f_{P1}, f_{P2}, f_{D1}, f_{D2}$ functions in thermal field	heat			
turbulence model	$\beta$ volumetric expansion coefficient			
G mass flux	$\varepsilon$ dissipation rate of turbulent kinetic			
$G_k$ production of turbulence due to	energy, $v(\partial u/\partial x_i)(\partial u/\partial x_i)$			
buoyancy	$\varepsilon_t$ dissipation rate of $\overline{t^2}$ , $\alpha(\partial t/\partial x_i)(\partial t/\partial x_i)$			
h enthalpy				
$k_t$ temperature variance, $t^2$	$\lambda$ , $\lambda t$ molecular and turbulent conductivity			
$k$ turbulent kinetic energy, $\overline{u_i u_i}/2$	$\mu$ , $\mu_t$ molecular and turbulent viscosity			
P pressure	$v$ , $v_t$ molecular and turbulent kinematic			
$P_k$ production of turbulence due to shear	viscosity, $\mu/\rho$ , $\mu_t/\rho$			
$P_t$ production of temperature variance	$\rho$ density			
Pr, Prandtl number	$\sigma_k, \sigma_{\varepsilon}, \sigma_{h}, \sigma_{\phi}$ model constants for turbulent			
q heat flux	diffusion of $k$ , $\varepsilon$ , $k_t$ , and $\varepsilon_t$ .			
r radial coordinate	$\sigma_{t}$ turbulent Prandtl number			
Re Reynolds number	au shear stress			
<i>Re</i> <sub>t</sub> turbulent Reynolds number				
T, t mean temperature and temperature	Subscripts			
fluctuation	c symmetry line			
<i>u, v</i> mean velocity and velocity fluctuation in	<i>e</i> effective (molecular + turbulent)			
x and $r$ direction	w wall			

# 7. References

- [1] A Technology Roadmap for Generation IV Nuclear Energy Systems, GIF-002-00, USDOE Nuclear Energy Advisory Committee and the Generation IV International Forum, December (2002).
- [2] X. Cheng, T. Schulenberg, 2001. "Heat Transfer at Supercritical Pressures—Literature Review and Application to an HPLWR," Wissenschaftliche Berichte (Tech. Report) FZKA 6609, Forschungszentrum Karlsruhe, Mai.
- [3] I. L. Pioro, R.B. Duffey, 2005. "Experimental heat transfer in supercritical water flowing inside channels (survey)," Nucl. Eng. Des. 235 (22), 2407–2430. Nov.
- [4] M. J. Watts, C. T. Chou, "Mixed convection heat transfer to supercritical pressure water" Int. Heat Transfer Conf. München 3 (1982) 495–500.
- [5] J. D. Jackson, W.B. Hall, "Influences of Buoyancy on Heat transfer to fluids flowing in vertical tubes under turbulent condition," in: S. Kakaç, D.B. Spalding (Eds.), Turbulent Forced Convection in Channels and Bundles, Hemisphere Publishing, 1979, pp. 613–640.
- [6] J.D. Jackson, M.A. Cotton, B. Axcell, "Studied of mixed convection in vertical tubes," Int. J. Heat Fluid Flow 10 (1) (1989) 2–15.
- [7] Y. Y. Bae, H. Y. Kim, "Convective heat transfer to CO2 at a supercritical pressure flowing vertically upward in tubes and an annular channel," Exp. Therm. Fluid Sci. Vol. 33, No. 2, 2009, pp. 329-339.
- [8] Y. Y. Bae, H. Y. Kim, D. J. Kang, "Forced and mixed convection heat transfer to supercritical CO 2 vertically flowing in a uniformly-heated circular tube," Experimental Thermal and Fluid Science 34 (2010) 1295–1308.
- [9] Y. Y. Bae, "Mixed Convection Heat Transfer to Carbon Dioxide Flowing Upward and Downward in a Vertical Tube and an Annular Channel," Proc. of 1 st Meeting of International Specialists on Supercritical Pressure Heat Transfer and Fluid Dynamics, University of Pisa, Pisa, Italy, July 5-8, 2010.
- [10] J.D. Jackson, "An extended model of variable property developing mixed convection heat transfer in vertical tubes," Proc. of 1st Meeting of International Specialists on Supercritical Pressure Heat Transfer and Fluid Dynamics, University of Pisa, Pisa, Italy, July 5-8, 2010
- [11] J. Licht, M. Anderson, M. Corradini, "Heat Transfer and Fluid Flow Characteristics in Supercritical Pressure Water," Journal of Heat Transfer July 2009, Vol. 131, 072502-1.
- [12] B. H. Cho, Y. I. Kim, Y. Y. Bae, "Prediction of a heat transfer to CO<sub>2</sub> flowing in an upward path at a supercritical pressure." Nucl. Eng. Tech., 41(7), 907-920, (2009).
- [13] S. He, W. S. Kim, J.D. Jackson, "A computational study of convective heat transfer to carbon dioxide at a pressure just above the critical value," Applied Thermal Engineering 28 (2008) 1662–1675.
- [14] H, Zhang, Z. R. Xie, Y. H. Yang, "Numerical Study on Supercritical Fluids Flow and Heat Transfer under Buoyancy," The 8th International Topical Meeting on Nuclear Thermal-Hydraulics, Operation and Safety (NUTHOS-8) paper No.: N8P0187, Shanghai, China, October 10-14, 2010

- [15] M. M. Gibson, "On the calculation of horizontal, turbulent, free shear flows under gravitational influence," J. of Heat Transfer, 98, pp 81-87 (1976).
- [16] K. Hanjalić, S. Vasić, "Computation of turbulent natural convection in rectangular enclosures with an algebraic flux model," Int. J. Heat Mass Transfer, 36(14), pp.3603-3624 (1993).
- [17] K. Abe, T. Kondoh, Y. Nagano, "A new turbulence model for predicting fluid flow and heat transfer in separating and reattaching flows—II. thermal field calculations," Int. J. Heat Mass Transfer, 38, pp.1467-1481 (1995).
- [18] H. K. Myong, N. Kasagi, M. Hirata, "Numerical prediction of turbulent pipe flow heat transfer for various Prandtl number fluids with the improved k- $\varepsilon$  turbulence model," JSME Int. J, 32, No. 4, pp.613-622 (1989).
- [19] K. Abe, T. Kondoh, N. Nagano, "A new turbulence model for predicting fluid flow and heat transfer in separating and reattaching flows—I: flow field calculation," Int. J. Heat Mass Transfer, 37, pp.139-151 (1994).
- [20] Y. Nagano, M. Tagawa, "An improved k- $\varepsilon$  model for boundary layer flows," J. Fluids Engng, 112, pp.33-39 (1990).
- [21] H. K. Myong, N. Kasagi, "A new approach to the improvement of the *k-ε* turbulence model for wall bounded shear flows," JSME Int. J, Vol. 33, No. 1, pp.63-72 (1990).
- [22] W. P. Jones, B. E. Lauder, "The prediction of laminarization with a two-equation model of turbulence," Int. J. Heat Mass Transfer, 15, pp.301-314 (1972).
- [23] D. R. Chapman, G. D. Khun, "The limiting behavior of turbulence near a wall," J. Fluid Mech., 170, pp. 265-292 (1986).
- [24] V. C. Patel, W. Rodi, G. Scheurer, "Turbulence models for near-wall and low Reynolds number flow: a review," AIAA J. Vol. 25, pp. 1308-1319 (1984).
- [25] J. Herrero, F. X. Grau, J. Grifoll, F. Giralt, "A near wall k-\varepsilon for high Prandtl number heat transfer," Int. J. Heat Mass Transfer, 34(3), pp. 711-721 (1991).
- [26] J. H. Ferziger, M. Peric, Computaional Metjhods for Fluid Dynamics, Springer-Verlag (1999).
- [27] J. H. Bae, J. Y. Yoo, H. Choi, "Direct numerical simulation of turbulent supercritical flows with heat transfer," Phys. Fluids, 17, paper No.105104 (24 pages) (2005).
- [28] E.W. Lemmon, M.D. McLinden, M.L. Huber, 2006. Reference Fluid Thermodynamics and Transport Properties. NIST Standard Reference Database 23, Version 7.1, Beta version.